Variability in the Deep Western Boundary Current: Local versus remote forcing

B. Peña-Molino,[1,2] T. M. Joyce,[1] and J. M. Toole[1]

Received 17 July 2012; revised 30 October 2012; accepted 31 October 2012; published 22 December 2012.

[1] Horizontal velocity, temperature and salinity measurements from the Line W array for the period 2004–2008 show large changes in the water mass structure and circulation of the Deep Western Boundary Current (DWBC). Fluctuations in the flow with periods from 10 to 60 days are bottom intensified: signals most likely associated with topographic Rossby waves (TRW). A fraction (∼15%) of the DWBC transport variability is caused by Gulf Stream rings and meanders. These flow anomalies are surface intensified and fluctuate at frequencies lower than the TRW. Interannual variability in the velocity field appears to be related to changes in the hydrographic properties. The dominant mode of variability is characterized by an overall freshening, cooling, a potential vorticity (PV) increase in the deep Labrador Sea Water (dLSW) and a PV decrease in the Overflow Water (OW). The variability in the flow associated with these property changes is not spatially homogeneous. Offshore (water depths larger than 3500 m) changes in the velocity are in phase with PV changes in the OW: a decrease in the OW PV is accompanied by an increase in the southward (negative) transport. Conversely, variations of the inshore flow are in phase with changes in the dLSW PV (increasing PV and decreasing transport). This trend, true for most of the record, reverses after the winter of 2007–2008. A sudden decrease of the dLSW PV is observed, with a corresponding intensification of the flow in the inner DWBC as well as a northward shift in the Gulf Stream axis.

Citation: Peña-Molino, B., T. M. Joyce, and J. M. Toole (2012), Variability in the Deep Western Boundary Current: Local versus remote forcing, *J. Geophys. Res.*, *117*, C12022, doi:10.1029/2012JC008369.

1. Introduction

[2] Dense water formation in the subpolar and subarctic basins has traditionally been thought to play an important role in the Atlantic Meridional Overturning Circulation (AMOC). In the *Stommel and Arons* [1960] idealized theory for the abyssal circulation of the ocean, localized sinking at high latitudes is balanced by homogeneously distributed upwelling. The resulting circulation in the interior, a poleward flow driven by the upwelling, is closed by an equatorward flowing current that is located along the western boundary due to vorticity constraints. The strength of the boundary current is directly related to the strength of the sinking, in that the boundary current is the only part of the circulation responsible for exporting dense water away from the formation sites. Although the Stommel-Arons theory was formulated for the steady circulation of the ocean, one might expect that changes in the dense water formation that occur over long time scales, as is the case for the dense water formed in the northern North Atlantic, will induce changes in the transport of the Deep Western Boundary Current (DWBC). However, with increasing evidence of the role that eddies and interior pathways play in the export of North Atlantic Deep Water (NADW) into the subtropics [e.g., *Bower et al.*, 2011; *Gary et al.*, 2011] whether or not changes in the DWBC can be linked to changes in the AMOC is yet to be determined.

[3] The properties as well as the formation rates of the dense water originating in the Labrador Sea, one of the most studied convection sites, are known to experience large fluctuations at interannual and longer time scales [e.g., *Lazier*, 1980; *Talley and McCartney*, 1982; *Yashayaev*, 2007]. The large heat fluxes (from the ocean to the atmosphere) that occur in the Labrador Sea during winter time are partly responsible for the densification of the surface water and the consequent overturn. However, as was noted by *Clarke and Gascard* [1983], freshwater fluxes and changes in the cyclonic circulation of the subpolar gyre can also play a crucial role. The deepest and strongest convection ever observed in the Labrador Sea occurred during the late 1980s and early 1990s [*Yashayaev*, 2007]. During this period, as well as during previous enhanced convection events, the North Atlantic Oscillation index (NAO) was large and positive. During the late 1990s, as the NAO entered a negative phase, deep wintertime convection ceased in the Labrador

[1]Woods Hole Oceanographic Institution, Woods Hole, Massachusetts, USA.
[2]Antarctic Climate and Ecosystems Cooperative Research Center, University of Tasmania, Hobart, Tasmania, Australia.

Corresponding author: B. Peña-Molino, Antarctic Climate and Ecosystems Cooperative Research Center, University of Tasmania, Private Bag 80, Hobart, Tas 7001, Australia. (beatriz.penamolino@utas.edu.au)

0148-0227/12/2012JC008369

Sea, and it was not until the early 2000s that convection restarted, but reaching to much shallower depths than the previous decade. This relationship between the NAO and the Labrador Sea Water (LSW) variability was clear in the *Curry and McCartney* [2001] LSW temperature record, with the temperature evolution of the Labrador Sea mirroring the NAO index.

[4] The return of deep convection to the Labrador Sea in the winter of 2007–2008 [*Våge et al.*, 2009; *Yashayaev and Loder*, 2009] suggests a more complex relationship between atmospheric forcing and convection than previous studies have shown. This recent reestablishment of the deep convection was described as "surprising" by *Våge et al.* [2009] due to the atypical conditions existing in the Labrador Sea during that winter. According to these authors, the relation between atmospheric forcing and the strength of convection is highly complex, and involves several other factors such as the sea ice distribution and the location of storm tracks. Hence, the chance of successfully predicting future deep convection events appears to be small.

[5] The formation rates and properties of the Overflow Water (OW), including Denmark Strait (DSOW) and Iceland-Scotland Overflow Water (ISOW) are also subject to interannual fluctuations [*Macrander et al.*, 2005]. However, the relation between changes in the OW and changes in the basin-scale atmospheric forcing has the opposite sense to that in the Labrador Sea. During high NAO periods, when convection is maximum in the Labrador Sea, the deep Nordic Seas grow progressively warmer and more saline due to weakened deep convection that in turn may be caused by an increase in the influx of low-density water of Arctic origin [*Dickson et al.*, 1996].

[6] Beyond the causes of deep convection variability in the northern North Atlantic, whether or not such changes in dense water formation can cause changes in the AMOC remains unclear at this point. The lack of long-term measurements, the different definitions of the overturning stream function, and the variety of model configurations make comparison of the available studies rather challenging. Of the two major constituents of North Atlantic Deep Water (NADW), the LSW and the OW, the relation between the latter and the AMOC inferred from observations and models (and between models themselves) appears the more robust. In *Gerdes and Köberle*'s [1995] model of the North Atlantic, an increase in the production of OW leads to a stronger DWBC and more vigorous meridional overturning. This result is in good agreement with *Koltermann et al.*'s [1999] findings whose analysis of hydrographic data from a series of repeated sections in the North Atlantic suggested that the dominant driver of the AMOC is the DSOW. Variations in the production of the LSW did not appear to have any effect on the strength of the AMOC. This same conclusion was reached by *Böning et al.* [1996] and *Kohl and Stammer* [2008] based on modeling experiments as well as by *Pickart and Spall* [2007] from both model and observations. It is also supported by *Schott et al.*'s [2006] temperature and velocity moored observations along the DWBC that showed a warming trend at the depth of the LSW with no significant long-term changes in the corresponding transports.

[7] The lack of a LSW contribution to the AMOC is however at odds with the meridional overturning stream function estimates by *Talley et al.* [2003] from hydrography-derived geostrophic and climatological Ekman velocities. Similarly, *Mauritzen and Häkkinen* [1999] found that a reduction in the formation of LSW can cause a decrease in the strength of the AMOC in their North Atlantic–Arctic coupled ocean ice model. The increase in the AMOC strength that follows periods of high NAO in the *Eden and Willebrand* [2001] modeling study further supports the role of the LSW in the AMOC, since high NAO is related to enhanced production of LSW.

[8] In recent years great progress has been made in monitoring the mean and variability of the MOC at 26.5°N as part of the Rapid-Meridional Overturning Circulation (RAPID) and Meridional Overturning Circulation and Heat Flux Array (MOCHA) programs. Their efforts have led to the first full-basin MOC observations and revealed that the MOC variability is large at a wide range of time scales, with a mean maximum transport around 18.5 Sv and standard deviation of approximately 5 Sv [e.g., *Cunningham et al.*, 2007; *Rayner et al.*, 2011]. Measurements along the western boundary have also shown that the variability in the transport of the DWBC at this location far exceeds that of the MOC [*Meinen et al.*, 2012], despite the remarkable coherence between changes in the water mass properties at 26.5°N and those observed in the northern North Atlantic (albeit a 9 year transit time [*van Sebille et al.*, 2011]). However, the relationship between the MOC at this and other latitudes is still unknown.

[9] Of the many studies described above many are based on records with a limited number of observations (thus strongly influenced by the ocean's eddy variability and not necessarily representative of the long-term changes) or poor resolution (and so cannot properly resolve the vertical structure of the changes associated with the production of the different constituents of NADW). The work presented here is based on a 4 year record of temperature, salinity and direct horizontal velocity measurements with both high temporal and spatial resolution. In this study we explore the variability in the water masses that are formed by convection at high latitudes as they are exported southward into the subtropical domain along the western boundary, and describe the changes in the western North Atlantic circulation that are associated with them. To do so it is necessary to separate signals originating at high latitudes from those locally forced. This is done in section 3 where a filter to extract Gulf Stream rings and meanders from the data set is developed, and section 4 where we take a look at the energetics of the flow, with special attention to the high-frequency signals. In the remainder of the paper we investigate the low-frequency changes in the circulation that correlate with changes in the water mass distribution in section 5, in section 6 we present transport estimates for the water masses that are well resolved by the array, and finally, in section 7, before the conclusions, we discuss an abrupt change in the circulation and hydrographic properties in the array that occurred toward the end of the record in the winter of 2007–2008.

2. The Data Set

2.1. The Line W Array

[10] The Line W record consists of a total of 5 moorings spanning the measurement period May 2004 to April 2008 (the moorings have been redeployed since, and results from

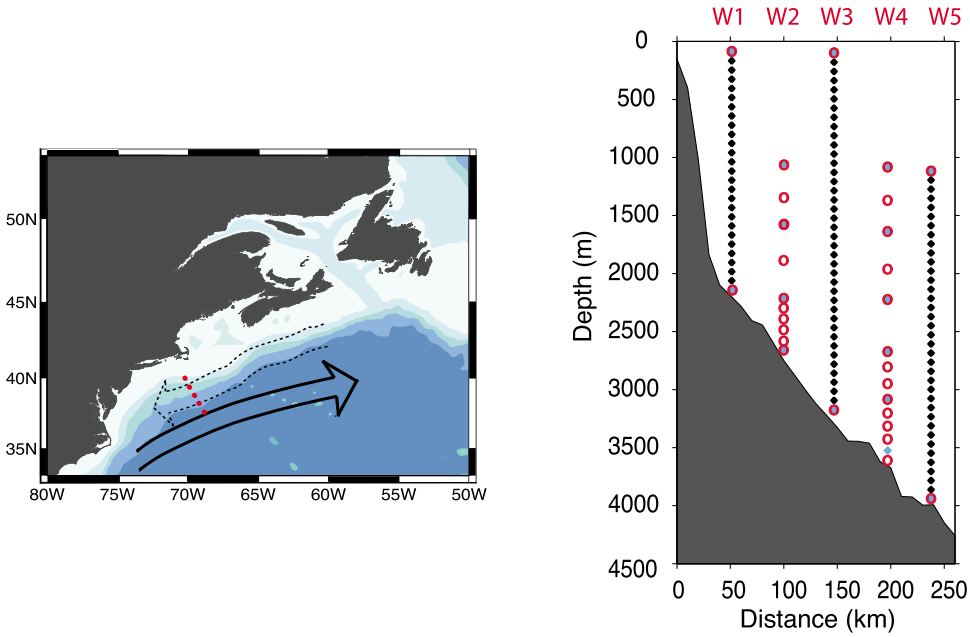

Figure 1. (left) Map of the location of the Line W array over the continental slope, indicated by the red dots. The dashed arrow indicates the mean southwestward flow in the DWBC, and the solid arrow indicates the mean Gulf Stream flow. (right) A schematic of the mooring setup. Moorings W1, W3 and W5 correspond to the MMP moorings. Black dots represent the MMP's profiling range. Blue dots and red circles represent the approximate location of the VACMs and MicroCATs respectively (moorings W2 and W4). For the exact depths, see Table 1.

the extended data set will be presented elsewhere). The array is located along the continental slope in the western North Atlantic at approximately 69°W 40°N (see location in Figure 1). The orientation of the array is 151° (clockwise from the North direction), approximately perpendicular to the local bathymetry in the area and the direction of the mean southwestward flow in the DWBC. Throughout this paper we will use the along-isobath direction as the nominal downstream direction, and thus the cross-stream direction parallels the array. The mean Gulf Stream intersects the array not quite perpendicularly, due to its slightly more zonal path.

[11] The array is a mixture of profiling moorings (denoted W1, W3 and W5 in Figure 1), equipped with McLane Mooring Profilers (MMP) measuring temperature, pressure, conductivity and horizontal velocity, and fixed depth sensor moorings (denoted W2 and W4), equipped with Vector Averaging Current Meters (VACM) measuring horizontal velocity and pressure, and MicroCATs measuring temperature and conductivity. The MMP moorings were also equipped with VACM and MicroCATs at the top and/or bottom of the MMP sampling ranges. The record consists of four 1 year deployments for the MMP moorings (higher battery demands requires more frequent servicing) and two 2 year deployments in the case of the fixed depth sensor moorings.

[12] The MMP data were binned during processing to a vertical resolution of 2 dbar, with the shallower moorings, W1 and W3, covering virtually the entire water column (from 100 m depth to approximately 50 m above the bottom), while the deepest of the moorings, W5 that sat near the Gulf Stream's North Wall, sampled between 1000 m and the bottom (~4500 m at this location; Figure 1). The MMPs were programmed to sample in bursts with each burst separated by 5 days and consisting of four one-way profiles. Averaging all four profiles in a burst effectively removes both tidal and inertial energy from the data [*Silverthorne and Toole*, 2009]. VACMs recorded vector averaged velocity estimates at 30 min interval while the MicroCATs were programmed to sample every 15 min. The fixed sensor records were subsequently filtered with a 2 day low-pass filter and subsampled daily. A summary of the instrument depths for all moorings is provided in Table 1. Both MMPs and VACMs are equipped with pressure sensors; hence, the data can be optimally mapped into a regular grid (details provided in section 2.2) according to the actual pressure rather than nominal depth, and any potential contamination from mooring blow down is eliminated at this stage. For a detailed discussion of the instrument setup and data processing, the reader is referred to *Toole et al.* [2011].

2.2. Constructing an Objectively Mapped Section

[13] The Line W array consists of both moorings with high vertical resolution and relatively low temporal resolution (W1, W3 and W5) and moorings with high temporal resolution and low vertical resolution (W2 and W4). To take advantage of both, we use a three dimensional (horizontal, vertical and time) objective mapping routine to interpolate the observations into 10 km × 20 m grid at daily resolution. The scheme minimizes the error in the interpolated data given some knowledge of the covariance matrices between observations and between observations and gridded data (a detailed derivation of the technique is given by *Wunsch* [2006]).

[14] The mapping of temperature and salinity is performed directly on anomalies (the time mean at each mooring location was removed) rather than full fields, since here our interest is

Table 1. Mooring Setup

Mooring	Latitude	Longitude	Depth (m)	Instrument Type	Instrument Depth (m)
W1	39°36.0′N	69°43.1′W	2242	MMP	60–2145
				VACM	55, 2126
				T/S	62, 2126
W2	39°13.0′N	69°26.7′W	2752	VACM	1031, 1631, 2224, 2677
				T/S	1031, 1331, 1631, 1927, 2224, 2318, 2411, 2536, 2646, 2677
W3	38°50.6′N	69°11.1′W	3248	MMP	60–3150
				VACM	50, 3203
				T/S	50, 3203
W4	39°25.5′N	68°54.0′W	3686	VACM	1043, 1644, 2241, 2688, 3234, 3575[a]
				T/S	1043, 1343, 1644, 1943, 2241, 2688, 2927, 3138, 3234, 3316, 3397, 3433, 3607
W5	38°4.4′N	68°40.0′W	4110	MMP	1000–4050
				VACM	1007, 4079
				T/S	1007, 4079

[a]No data available for the first 2 years of the record for this instrument.

the variability and gridding the full fields would overly smooth the background stratification. However, in calculating transports full (mean plus variability) temperature and salinity sections are required to define the water mass interfaces. These mean sections are obtained by combining the mooring data with CTD and direct velocity measurements collected along Line W during the moorings deployment and recovery cruises. The hydrographic sections are fundamental in constructing the mean sections, since they have much finer vertical and horizontal resolution than the moorings and so provide information about the smaller scales. The differences between the time mean profiles from the moorings alone and the gridded mean sections at the moorings locations are on the order of <0.01°C for temperature and <0.001 for salinity (the ratio between them is related to the ratio of a typical δT to a typical δS, that is to the slope of the mean T/S curve). The errors in the water mass interface calculation associated with these differences are smaller than the vertical resolution of the objectively mapped data and therefore negligible for practical purposes.

[15] The gridded downstream and cross-stream velocity anomalies, on the other hand, are obtained by first mapping daily estimates of the full velocity field, and then computing and removing the time mean. Unlike temperature and salinity, the observed mean velocity field at Line W has little vertical variation [*Joyce et al.*, 2005; *Toole et al.*, 2011] and so the mean velocity does not affect the mapping. The resulting velocity anomalies are the same whether the time mean is removed before or after the mapping.

[16] The covariance matrices required by the method are chosen to be Gaussian functions of the distance (in the three-dimensional space: x, z and t) between each pair of points given some correlation lengths (σ_x, σ_z, and σ_t). Our choice of correlation scales is based on two factors: first, the typical scales of the variability, and second, the spacing between observations. Spatial scales for all variables are chosen based on the Line W hydrographic sections (typical station spacing 10–20 km). From these data we find that the horizontal scales of temperature, salinity and velocity anomalies are typically on the order of 100 km. Vertical correlation scales for temperature and salinity anomalies are found to be 500 m or larger. In the case of the velocity, the fluctuations are coherent through the water column. Based on these scales, the array design, with typical horizontal resolution of 50 km and vertical spacing between fixed depth sensors of 100–500 m, is not limiting. In order to minimize the misfit between the original data and the objectively mapped product (the longer the scales employed in the mapping, the smoother the final product, and so the larger the misfit) we use a 60 km horizontal correlation scale and a 500 m vertical correlation scale. These scales may appear seemingly large for the Gulf Stream, but they are appropriate for the Slope Water and DWBC to the north.

[17] The uncertainty provided by the mapping method is a function of the correlation scale itself; the larger the scales the smaller the uncertainty, so it should not be interpreted as a true error, but as guideline to discard mapped data in regions that are poorly sampled. To obtain an estimate of the misfit associated with the selected length scales and array design, we subsampled the hydrographic sections using the mooring sampling scheme and then objectively mapped them back on to the original grid. Doing this we find upper bounds for the magnitude of the misfit (in the RMS sense) of 0.002 m s^{-1} for the velocity, 0.01°C in temperature and 0.0005 in salinity. If the top 1000 m of the water column, where the mooring array does a poor job sampling, are excluded, the amplitude of the temperature and salinity misfit is 1 order of magnitude smaller.

[18] Decorrelation time scales are obtained from the fixed depth sensors in the moorings. The obtained values ranged from 50 and 100 days, and are strongly controlled by the frequency of rings in the records. Using these decorrelation times leads to a very smooth field and made for a more computationally expensive calculation. In the absence of rings and meanders, decorrelation times are much smaller, typically 15–20 days. Based on the temporal resolution of the data (5 days for the MMP moorings, daily for the fixed sensors), the final product was obtained using a 7 day correlation scale. RMS errors based on the temporal correlation scale are similar to those associated with the spatial mapping.

[19] The analysis presented here only makes use of the well-resolved areas of the mapped fields, where uncertainties in the mapping are smaller than 10%. Regions with larger uncertainties are excluded.

3. Rings, Meanders and the Mean Circulation at Line W

[20] The upper part of the southernmost mooring at Line W, W5, is frequently embedded in the deep-reaching flank

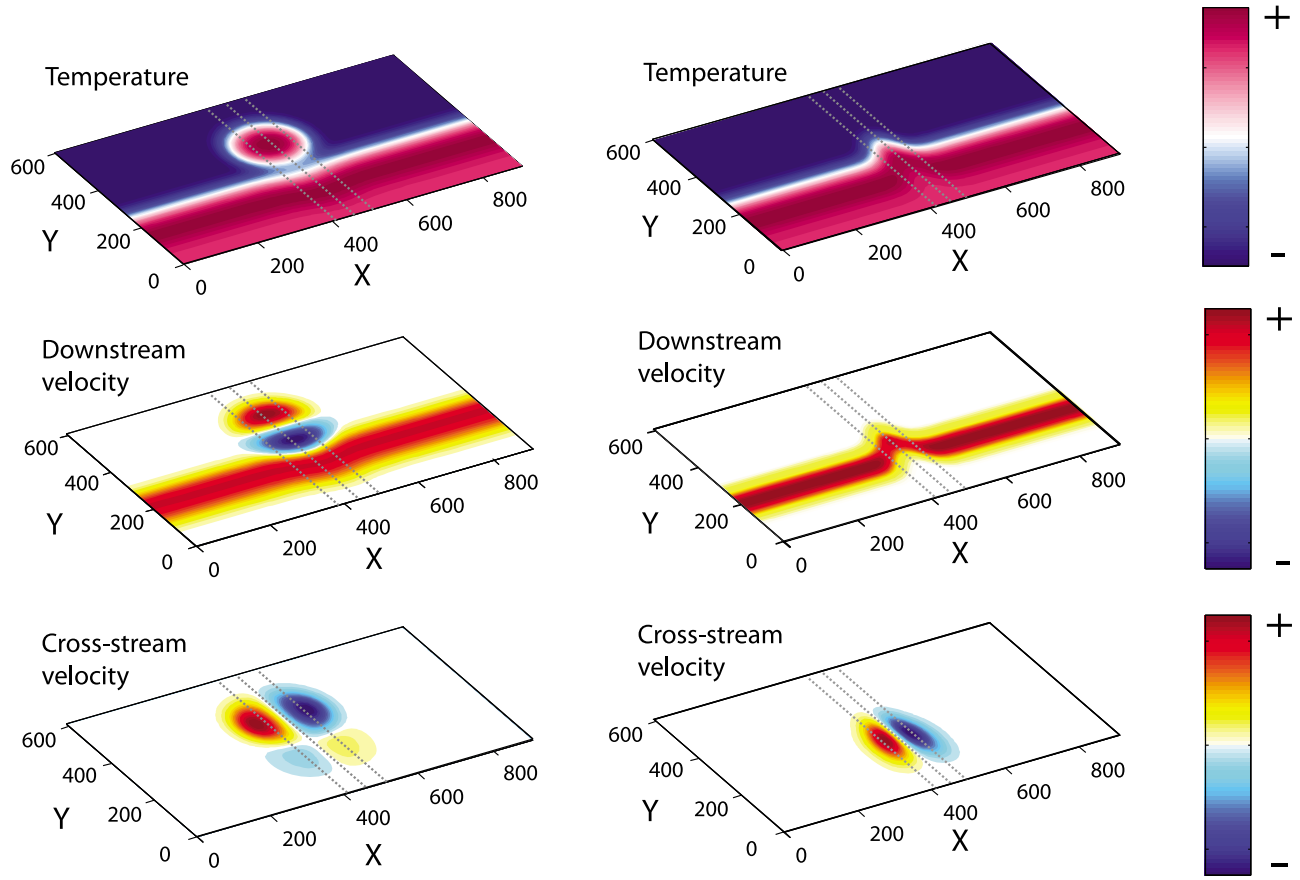

Figure 2. Surface views of the temperature, downstream and cross-stream velocity fields for (left) the idealized rings and (right) meanders. The gray dashed lines represent the location of a hypothetical section across the perturbation west of the center, at the center, and east of the center of each anomaly.

of the Gulf Stream, with typical velocities of about 5 cm s^{-1} (to the northeast). Because the horizontal gradients in the Gulf Stream's velocity core are large, even small fluctuations in the position of the Gulf Stream can produce large changes in the observed velocity at W5. These fluctuations are often associated with the baroclinically unstable nature of the Gulf Stream that leads to the formation of rings and meanders [e.g., *Cronin and Watts*, 1996]. Large rings and meanders can also be felt by the shallower moorings along Line W. The density contrast between the Slope Water and the Gulf Stream is also large, so both the density and velocity fluctuations associated with Gulf Stream rings and meanders are responsible for a significant fraction of the variability in the Slope Water [*Csanady and Hamilton*, 1988]. In fact, the dominant mode of variability in the velocity and temperature record at Line W is the presence/absence of warm rings and meanders. Throughout the record these warm type of anomalies were far more frequent and larger in amplitude than their cold counterparts, and so our analysis focuses on them. In order to investigate the inherent variability of the DWBC, with amplitudes 1 order of magnitude smaller than the fluctuations caused by the Gulf Stream, we need to exclude those periods in the record that are affected by rings and meanders.

[21] Gulf Stream rings and meanders exist at a large range of periods and wavelengths [e.g., *Watts and Johns*, 1982; *Brown et al.*, 1986]. They can migrate or be stationary for long periods and although they are frequent, filtering the record for a particular frequency band does not ensure their complete elimination. Moreover, such treatment will most likely eliminate other signals of interest within the same frequency band. Instead, our approach to eliminate rings and meanders from the time series is to construct an index based on a idealized representation of the Gulf Stream as a baroclinic jet with a Gaussian velocity core that follows a linear path. The jet is in geostrophic balance, so there is an associated horizontal density gradient, with the warm Sargasso Sea water to the south, and the colder Slope Water to the north. This rectilinear jet represents the Eulerian time mean Gulf Stream. The density and velocity anomalies associated with the passing of rings and meanders are calculated as the difference between the synoptic (perturbed) field and the mean linear jet. This highly simplified representation of the Gulf Stream path variability does not account for changes in the jet's vertical structure [e.g., *Shay et al.*, 1995; *Lindstrom and Watts*, 1994] or the asymmetry in the relative vorticity to either side of its core [e.g., *Rossby and Gottlieb*, 1998], but it is nevertheless sufficient for the purpose of this study.

[22] Gulf Stream meanders are lateral shifts of the entire baroclinic structure of the jet [e.g., *Watts and Johns*, 1982; *Halkin and Rossby*, 1985], and so we model them as Gaussian perturbations to the path. Warm core rings (WCR), on the other hand, are generated when large north extending meanders detach from the main stream [e.g., *Joyce et al.*, 1983; *Brown et al.*, 1986] leading to clockwise rotating structures

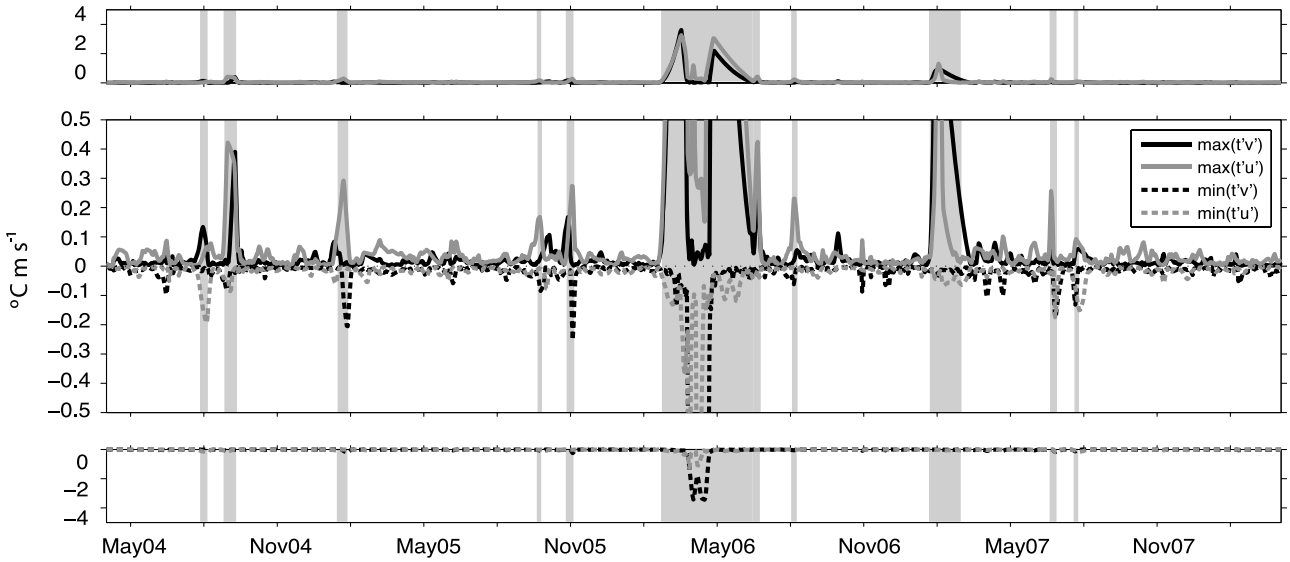

Figure 3. (top) Time series of max($T'v'$) in solid black, max($T'u'$) in solid gray. (bottom) Time series of min($T'v'$) in dashed black and min($T'u'$) in dashed gray. (middle) All four time series at the vertical scale of the typical perturbations. The event in the spring-summer of 2006 was 1 order of magnitude larger. Periods that exceeded the filter's threshold as defined in section 3 are shown by the gray shaded areas.

with surface velocities at times as large as 2 m s^{-1}. Thus they may be represented as circular perturbations with the same baroclinic structure as the linear jet, but separated from it (Figure 2).

[23] Both rings and meanders displace warm Sargasso water to the north, into the much colder Slope Water. As a result, regardless of where a section crosses a Gulf Stream perturbation, it will always have large positive temperature anomalies associated with it. On the other hand, the sign and amplitude of the downstream (u') and cross-stream (v') velocity anomalies associated with a Gulf Stream ring or meander, will depend upon where the hypothetical section crosses the perturbation: upstream (west) from the center or downstream (east) from the center (right at the center the cross-stream velocity is zero). Four possible scenarios can occur in a section north of the mean Gulf Stream that is affected by a ring or meander. Defined as combinations of temperature and downstream velocity anomalies, $T'u'$, and temperature and cross-stream velocity anomalies, $T'v'$, these scenarios are: ($T'u' > 0$ or $T'u' < 0$, $T'v' > 0$) for a section intersecting a ring to the west of the ring's center, ($T'u' > 0$ or $T'u' < 0$, $T'v' < 0$) for a section intersecting a ring to the east of the ring's center, ($T'u' > 0$, $T'v' > 0$) for a meander intersecting a meander to the west of the meander's peak and ($T'u' > 0$, $T'v' < 0$) for a section intersecting a meander to the east of the meander's peak.

[24] The amplitude of the velocity and temperature anomalies caused by rings and meanders is much larger than the inherent variability of the Slope Water. Thus by searching for extreme occurrences of $|T'u'|$ and $|T'v'|$ combinations in the section we can determine when the array was affected by a ring or meander. These extreme anomalies, like the large property gradients in the Gulf Stream they originate from, tend to be found in the upper part of the water column. However, where in the section the extrema occurs is irrelevant; it is the presence or absence of large values that we are after.

[25] Time series of maxima and minima of $T'u'$ and $T'v'$ for the objectively mapped Line W data in Figure 3 shows a very large WCR event in the spring-summer 2006. Both its amplitude (1 order of magnitude larger) and duration (8% of the length of the Line W time series) are unique in the record. Sea surface temperature (SST) snapshots during this event confirm both the scale and persistence of this feature (Figure 4). Several other smaller events are seen in the time series as well, and can be identified in the SST field (not shown here). We define ring/meander events as those that exceed 0.1°C m s^{-1}, equivalent to a 10 cm s^{-1} velocity perturbation times a 1°C temperature perturbation: values that are typically seen in the Slope Water. Using this value, 15% of the record is affected by rings and meanders and is excluded from subsequent analysis (shown as gray shaded areas in Figure 3). Increasing or decreasing the value of the threshold by a factor of 2 has little impact on the percentage of filtered data.

[26] Once rings and meanders are excluded from the record, the resulting mean downstream velocity section (Figure 5) shows three distinct velocity cores to the north of the northeast Gulf Stream flow at W5: a shallow one centered at W1 at a depth of 1000 m, and two bottom-intensified cores located at the base of W2 and W4, respectively. Each of these cores has mean velocities of several centimeters per second to the southwest. Observations of the DWBC both upstream (east of the Grand Banks [e.g., *Schott et al.*, 2004]) and downstream (e.g., *Pickart and Smethie* [1993] at Cape Hatteras and *Schott et al.* [2005] at 5–11°S) from Line W also showed bottom intensified flow. However, no evidence of a boundary-intensified velocity core at the level of the uLSW (1000 m) was found by *Bower and Hunt* [2000] based on float observations, possibly a consequence of the lower vertical resolution of their data compared to ours and the smaller number of velocity estimates that went into their averages.

[27] These Eulerian mean velocities, integrated out to the maximum of the southwestward stream function for the deep

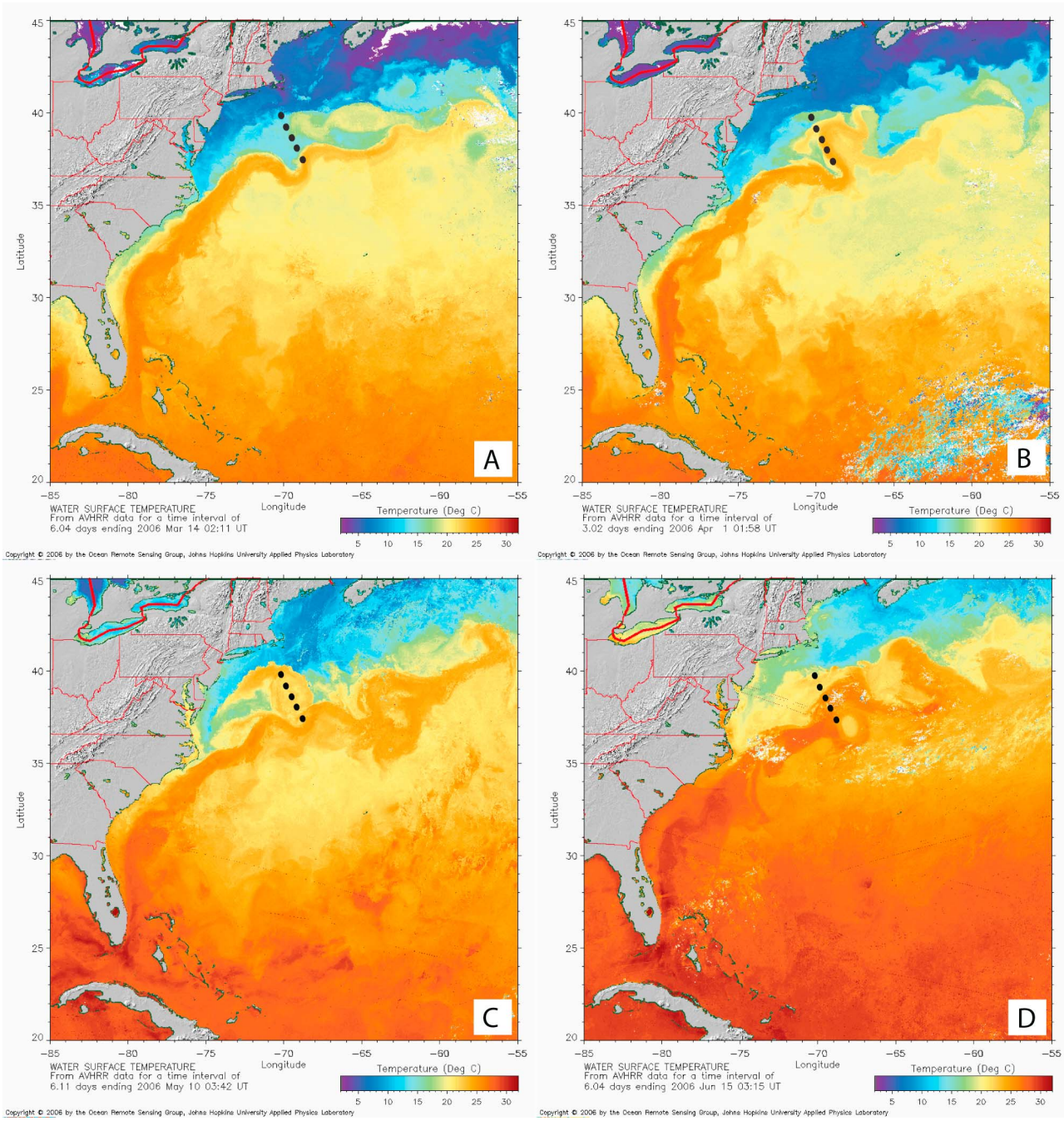

Figure 4. Snapshots of sea surface temperature (SST) (a) on 14 March 2006 before the ring develops, (b) on 1 April 2006 during the onset, (c) on 10 May 2006 when the ring is fully developed, and (d) on 15 June 2006 when the ring is being reabsorbed by the Gulf Stream. The location of the Line W mooring array is shown by the black dots. Figures made available by the Ocean Remote Sensing Group, Johns Hopkins University Applied Physics Laboratory (http://fermi.jhuapl.edu/avhrr/gs_n/index.html).

and intermediate water masses that are well resolved by the array, which are dLSW (between the 27.897 and 27.983 kg m^{-3} neutral density surfaces), ISOW (27.983–28.066 kg m^{-3}) and DSOW (28.066–28.125 kg m^{-3}), yield mean transport values of −6.8 Sv, −5.5 Sv and −5.5 Sv for each of the layers, respectively. These mean transport values are slightly smaller than those obtained by *Toole et al.* [2011], most likely due to differences in the mapping techniques. The uLSW, bounded by the 27.800 and 27.897 kg m^{-3} neutral density surfaces, is only partially resolved by the array, so it is excluded from this analysis.

[28] The mean cross-stream velocity section is slightly divergent. Near the bottom where the flow is steered by bathymetry, the divergence is caused by the spreading of the isobaths upstream of the array. Higher up in the water column, the flow transitions from being topographically steered, i.e., roughly perpendicular to the array (the nominal downstream direction), to a more zonal orientation paralleling the

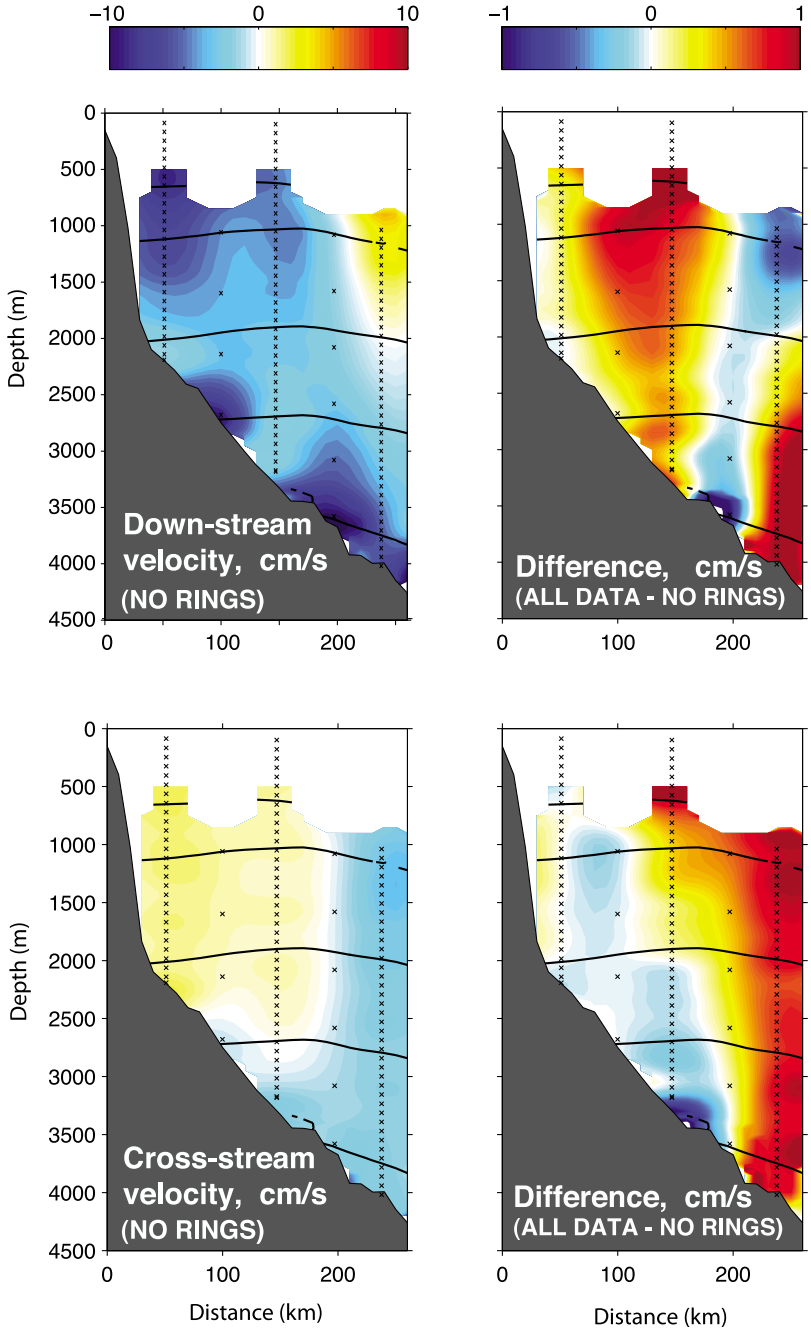

Figure 5. (left) Downstream and cross-stream mean velocity sections for the ring/meander filter record (on a scale of − 10 cm s^{-1} to 10 cm s^{-1}). (right) The difference between the mean velocity calculated with the full record, rings and meanders included, and the mean from the ring/meander-free record, for (top) the downstream velocity and (bottom) cross-stream velocity. Difference plots are on a scale of −1 cm s^{-1} to 1 cm s^{-1}. The solid black lines represent the interfaces between uLSW, dLSW, ISOW and DSOW. Black crosses indicate the location of the moorings.

mean Gulf Stream axis (a negative cross-stream component coordinate to our rotated axis).

[29] Comparing the mean downstream velocity section when all data are included versus that constructed after rings/meanders are excluded (Figure 5), we find that the rings effectively reduce the southward mean transport across the array by about 10% (approximately 0.5 Sv within each layer). The flow that is blocked by the rings/meanders, must be deflected to a different path. The deep components of the flow, are most likely deflected offshore. The shallow components, on the other hand, being confined to the north by the Gulf Stream, can only be diverted to an onshore path (unlikely due to the rapid shoaling of the bottom in this direction), or recirculate to the northeast after colliding with a ring/meander. The latter was the case in the *Bower and Hunt* [2000] float observations.

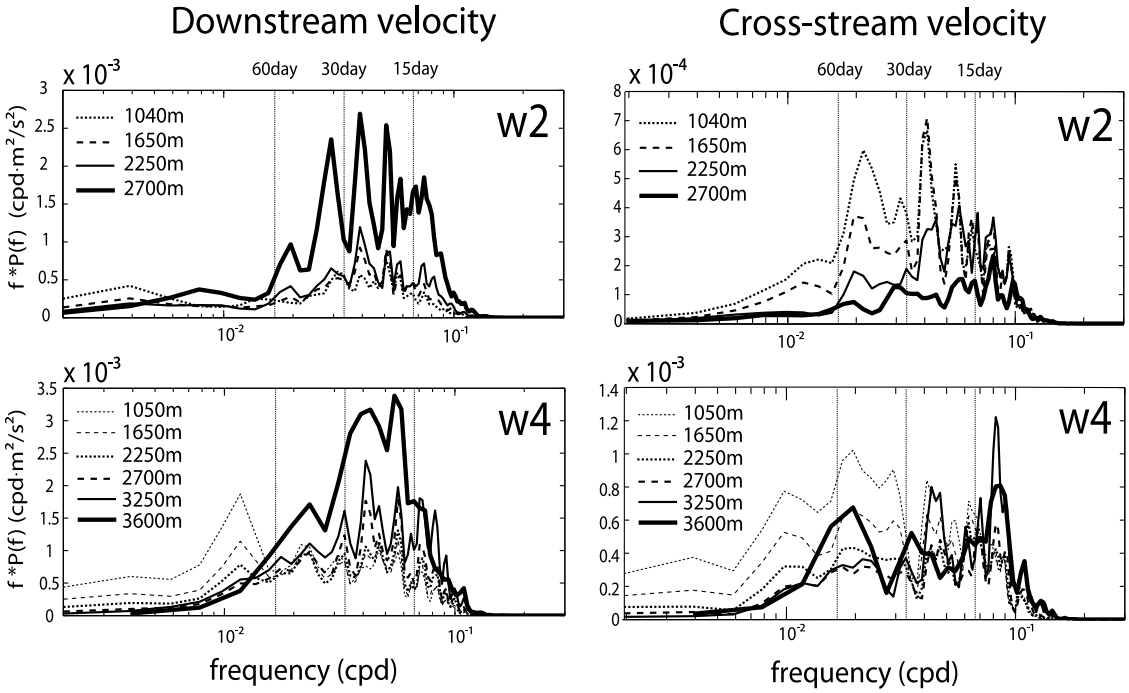

Figure 6. Frequency spectra of the (left) downstream and (right) cross-stream components of the velocity for moorings W2 and W4 (each plot has different vertical axis scale). Increasing instrument depth is denoted by increasing line thickness as indicated in the legends.

[30] In the cross-stream component, most of the contribution by rings is located at the offshore end of the section, the region that is directly affected by the Gulf Stream. The difference implies a reduction in the cross-stream component and it is the result of the somewhat more frequent occurrence (1.5 times more frequent) of a $T'v' > 0$ type of crossing (the section intersects the ring or meander to the west of its center) than a $T'v' < 0$ type (the section crosses to the east of the center of the ring/meander) events (see Figure 3).

4. Energetics of the Flow

[31] To characterize the distribution of fluctuating energy, we calculate frequency spectra of the 5 day (the common sampling period of all the instruments in the array) low-pass-filtered downstream and cross-stream velocities from the original velocity records at moorings W2 and W4 (those equipped with VACMs) (Figure 6). The spectra include all available data, with rings and meanders. The gappy nature of the ring-edited time series prevents us from using classical Fourier analysis.

[32] The downstream component of the velocity fluctuations appears to be bottom intensified for periods shorter than 60 days (Figure 6, left). For periods longer than 60 days, surface motions in the downstream direction are more energetic than motions at deeper levels. In general, energy increases with distance offshore, with W4 being almost twice as energetic as W2. Away from the bottom, W4 shows enhanced energy levels around the 100 day period. This same period has been previously associated with fluctuations in the transport of the DWBC [*Pickart*, 1994].

[33] Spectra of the cross-stream component of the velocity (Figure 6, right) shows quite a different picture. Overall, cross-stream motions are less energetic than the downstream motions by roughly a factor of 2 but more energetic in the upper part of the water column than at depth for the entire frequency range, contrasting with the bottom intensified nature of the higher frequencies for the downstream component.

[34] This asymmetry in the energy distribution of along-isobath and across-isobath motions at different frequencies was already noticed by *Thompson* [1971] and *Thompson and Luyten* [1976]. Their analysis of moored velocity records in the vicinity of the Gulf Stream highlighted two aspects of the flow variability in the area: (1) the flow near the bottom is principally in the along-isobath direction and (2) the principal axis of the velocity fluctuations depends on frequency. They found that motions at longer periods tend to run back and forth along isobaths, intermediate-frequency oscillations fluctuate in the across-isobath direction, and motions at higher frequencies tend to be isotropic. Our calculation does not resolve the high-frequency range in Thompson and Luyten's discussions, but the same relation between low and intermediate frequencies appears to be true here. In Thompson's work, motions with energy concentrated around periods of 1 week were linked to the passing of topographic Rossby waves (TRW). There are several observations of TRW over the continental slope in the western North Atlantic [e.g., *Pickart and Watts*, 1990; *Pickart*, 1995; *Fratantoni and Pickart*, 2003]. The range of frequencies that are often linked in the literature to TRW is somewhat broad. However, considering that according to quasi-geostrophic theory, the frequency of TRW depends on the topographic slope as well as the stratification, and both can be different in different parts of the western North Atlantic, a broad range of frequencies is to be expected.

[35] As to what excites TRW, *Pickart* [1995] argued they can be caused by Gulf Stream instabilities. Both TRW and Gulf Stream instabilities appear to be important sources of

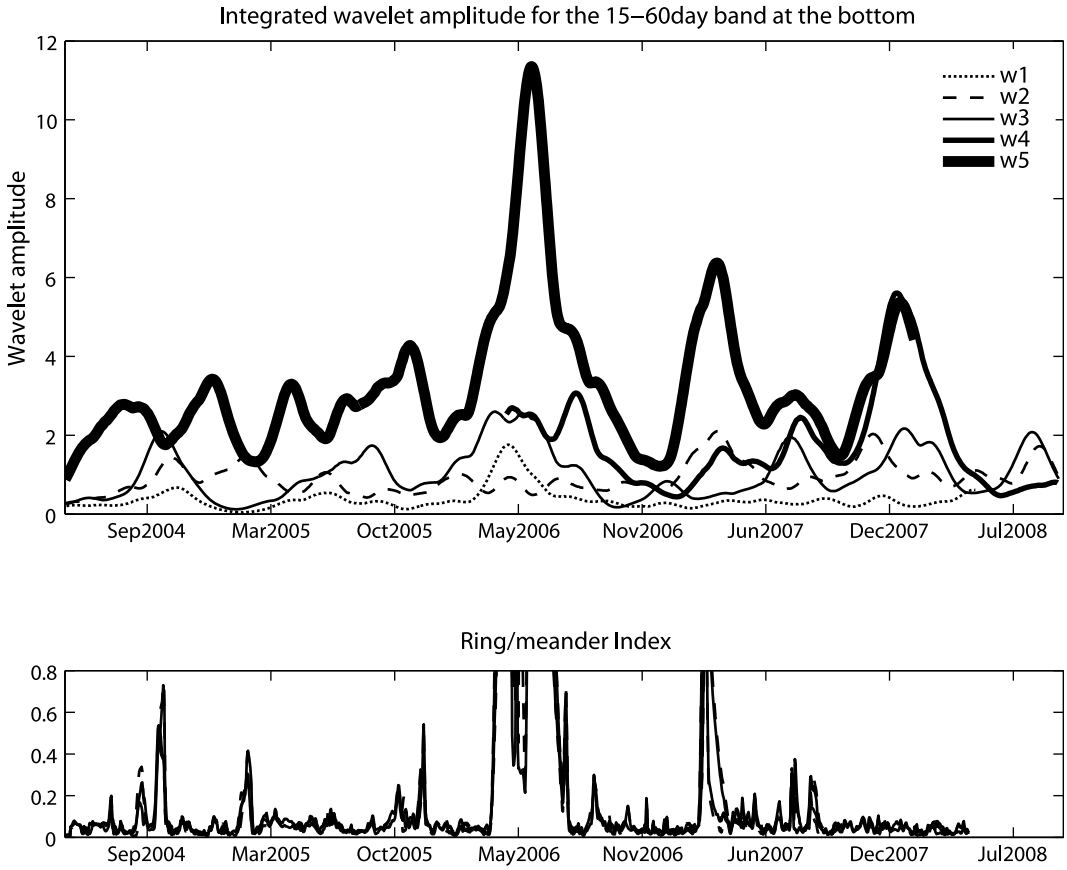

Figure 7. (top) The integral of wavelet amplitude for the 15–60 day band for the bottom current meters as a function of time. (bottom) The four combinations of temperature and velocity anomalies that characterized periods of time when the array is affected by rings and/or meanders as defined in section 4.

variability in our record. If the occurrence of TRW is related to the ring/meander activity of the Gulf Stream, the temporal evolution of the energy in the TRW frequency band, and the Gulf Stream ring/meander index from section 3 should show similar behaviors. We explored this relation by means of wavelet analysis (we used a complex Morlet wavelet function; for details on this and other aspects of wavelet analysis the reader is referred to *Torrence and Compo* [1998]). The analysis is restricted to the bottommost observations, both because motions below 1000 m appear to be bottom intensified in the array, and for practical reasons, since all moorings, including profiling moorings, were equipped with VACMs at the bottom (so instrumental differences were not an issue).

[36] In order to establish the relationship between the total energy content within the intermediate-frequency band typical of TRW and the presence or absence or rings and meanders in the array, we integrate the wavelet amplitude between the 15 day and the 60 day periods (Figure 7, top) and compare it to the temperature and velocity anomaly combinations described in section 3, expressed now as sums and differences as follows: $\max(T'u') - \min(T'u') + \max(T'v')$ for a section intersecting a ring to the southwest of the ring's center, $\max(T'u') - \min(T'u') - \min(T'v')$ for a section intersecting a ring to the northeast of the ring's center, $\max(T'u') + \max(T'v')$ for a meander intersecting a meander to the southwest of the meander's peak and $\max(T'u') - \min(T'v')$ for a section intersecting a meander to the northeast of the meander's peak (Figure 7, bottom). The integral of the wavelet amplitude shows that the energy increases offshore, as noted before. The most energetic features in the records appear to be associated with Gulf Stream rings and meanders, consistent with *Pickart*'s [1995] ideas on the generation of TRW by Gulf Stream instabilities, with the exception of a peak during the winter of 2007–2008 observed in W3, W4 and W5. This event is discussed in more detail in section 7.

5. Water Mass Changes and the Circulation Response

[37] Winter time convection at high latitudes produces water masses that are, in general, cold due to the large heat fluxes, fresh due to the mixing with low-salinity surface water and weakly stratified due to the convective mixing process. This low stratification, and therefore low potential vorticity (PV, here defined as $-(f/\rho_0)\partial\rho/\partial z$), may be used as an indicator of the intensity of convection, both inside and outside the convective basin: the more vigorous the convection, the lower the PV signal in the resulting water mass. When convection is weak or it does not occur, the water gradually restratifies causing the PV to rise [*Talley and McCartney*, 1982]. Elimination of the contribution from rings and meanders to the variability of the temperature,

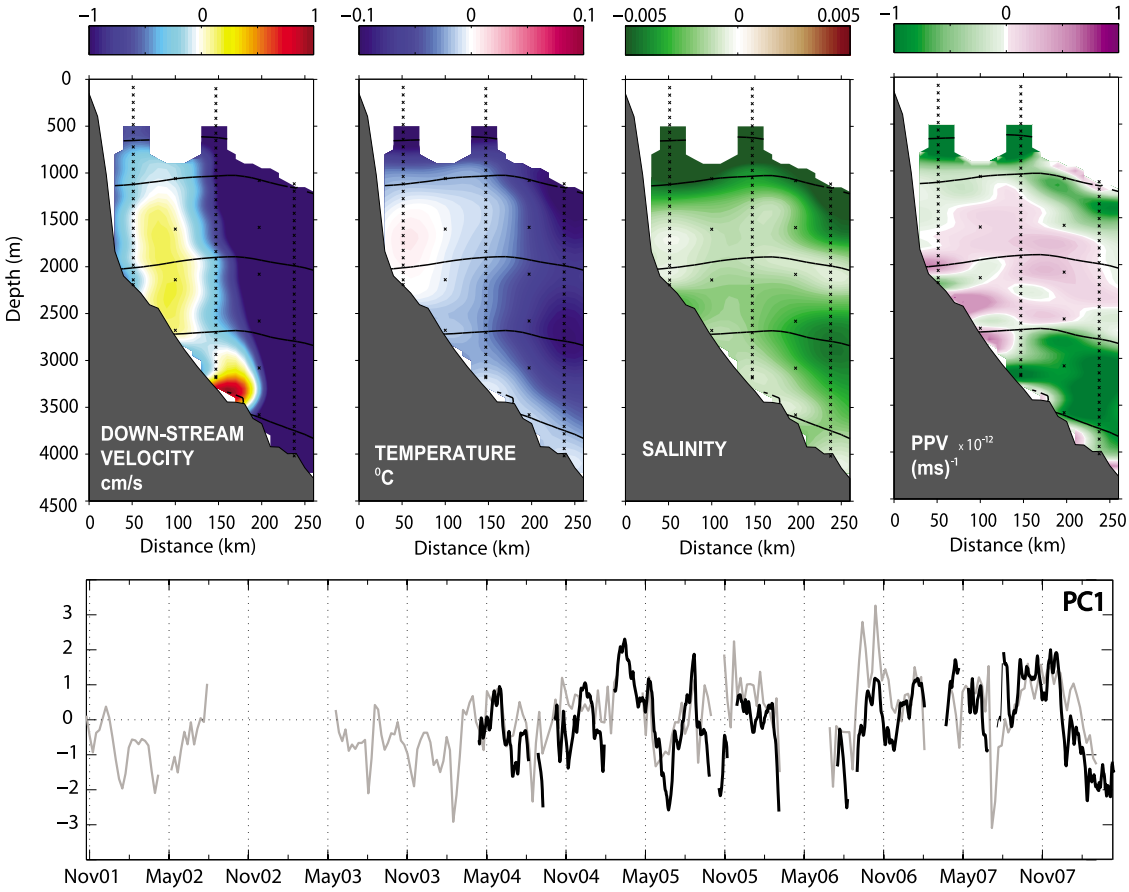

Figure 8. (top) Leading mode of the joint EOF of the downstream velocity, potential temperature, salinity and PPV, from left to right. The black contours represent the interfaces between upper LSW, deep LSW, ISOW and DSOW, from top to bottom. (bottom) The corresponding principal component (in black), and the leading principal component (in gray) of the joint EOF analysis from the W3 record from *Peña-Molino et al.* [2011] (both normalized).

salinity and velocity fields in our record allows us to detect changes in the water masses (cooling, freshening and decreasing PV) that may be linked to changes in dense water formation.

[38] To investigate changes in the circulation of the DWBC that are related to changes in dense water formation we calculate the joint EOF of the velocity, PV, temperature and salinity anomalies (time mean removed). By doing so we can extract the fraction of the variability in the velocity field that is correlated with changes in the water mass properties. The leading mode of the joint EOF analysis of the ring/meander-free time series (Figure 8) represents 20% of the variance of the combined fields. The percentage is not high, but the eigenvalues of the analysis are well behaved (they decay exponentially and are separated from successive modes by at least half their value [*North et al.*, 1982]) and considering that the analysis includes four independent variables with their corresponding noise, 20% is certainly not insignificant. Despite our effort to remove them, the influence of rings and meanders is still present in the trimmed record, distributed in higher modes with a nearly barotropic velocity pattern that fluctuate at periods of several days to a few weeks.

[39] The spatial structure of the PV mode shows a distinct layering pattern, with a positive PV anomaly at intermediate depths occupying the depth range of the dLSW and upper part of the ISOW, and negative PV anomalies above and below, in the uLSW and DSOW layers. These anomalies are laterally coherent across the section. During the phase when the PV anomaly is positive at the level of the dLSW (when PC1 > 0) the section is fresher and colder everywhere except for a small region at middepth in the vicinity of W1 where some weak warming is indicated. This warm core is only partially compensated by salinity, since there is no actual increase in the salinity at that location, only a weaker freshening, and is probably related to changes in the LSW core properties. Taking the PV signal as an indicator of ventilation for the LSW, our section is consistent with *Dickson et al.* [1996] finding of coordinated changes in convection in the Labrador and Nordic Seas. They found that during phases of deep convection in the Labrador Sea (corresponding to times when PC1 < 0 in our analysis), due to increased exchange with the Arctic, only shallow convection occurs in the Nordic Seas, leading to progressively warmer and more saline OW. However, this warming tendency is not exclusive to the deep layers at Line W but affects most of the water column, with

the exception of the temperature core at W1 mentioned earlier. It was shown in *Peña-Molino* [2010] that part of this depth independent salinity and temperature change is caused by the rising of the isopycnals associated with the expansion of the OW layer rather than changes in the properties of the water masses.

[40] The velocity signal that accompanies these changes in PV, temperature and salinity described above, consists of a large negative anomaly (values ranging from -5 to -10 cm s^{-1}) in the deep part of the section, a weaker positive anomaly (maximum values of 1 cm s^{-1}) in the shallow region below 1000 m centered at W2, and a larger positive core near the bottom at W3. The positive anomaly at W2 is isolated from the uLSW layer on top, where changes in the velocity are in phase with changes in the offshore part of the section. The amplitudes of the positive anomalies are small compared to the mean downstream flow in this part of the array. During positive phases (PC1 > 0), these anomalies act to decrease the southwestward mean flow, and during negative phases, they reinforce it. The effect of these anomalies in the transport integrated across the section will be discussed in section 6.

[41] PC1 shows frequent reversals throughout the record (Figure 8, bottom), but we find that on average PC1 was negative pre-2006, thus negative PV at intermediate depths, and positive after, with negative PV in the upper and deeper layers. This tendency is further supported by comparing PC1 to the principal component obtained in a similar analysis done by *Peña-Molino et al.* [2011] with a longer record from the central mooring, W3, of this array. The overall trend in their analysis [*Peña-Molino et al.*, 2011, Figure 3], is much more clear.

6. Intermediate and Deep-Water Transport

[42] In section 5 we showed that changes in the water mass structure at Line W are accompanied by changes in the amplitude, direction and spatial structure of the flow. In this section we explore the effect of these changes on the equatorward transport of the DWBC. We do so by first considering the fluctuations in the downstream component of the velocity (this is the direction of the mean flow in the DWBC and the cross-stream component does not contribute to the transport normal to the array) as calculated from EOF1, and compare them later to the total transports derived from the full time series.

[43] The transport response to changes in formation and export of deep and intermediate water masses along the DWBC is calculated by combining the joint EOF downstream velocity mode and mode-derived density variability with the velocity and density mean sections. The mean density section is only required to calculate the interfaces between the different water masses, and so the errors due to the difference in the mapping of T/S means and T/S variability are negligible, as discussed earlier. The downstream velocity, given by the sum of the EOF1 velocity mode and the mean velocity section, is then integrated across each layer out to the maximum in the transport stream function (only the equatorward flow). The position of the stream function maximum in this calculation depends only on the location of the Gulf Stream's North Wall, due to the fact that the velocity anomalies from the EOF mode are never large enough to reverse the southwestward mean flow.

[44] The changes in the density field and the circulation captured by the joint EOF analysis show a relatively barotropic response in the transport (Figure 9, top). DLSW, ISOW and DSOW transports appear to fluctuate in phase. There are three possible variables that contribute to the fluctuations in the transport: (1) the averaged layer velocity, (2) the offshore extension of the layer (given by the location of the stream function maximum) and (3) the averaged layer thickness. Changes in 1 and 2 are in phase for all three water masses, and are responsible for the bulk of the changes in the transport, as noted by *Toole et al.* [2011], hence its barotropic nature. Layer thickness changes, on the other hand, are different for each layer. However, their contributions to the total variations in transport are small. Overall, EOF1 is responsible for variations about the mean of approximately 5 Sv in each layer. There are clear year-to-year differences in the time series, with the maximum transports occurring during the spring of 2005 and fall of 2007, but no appreciable trend. Toward the end of the record, there is a rapid decrease in the transport of about 15 Sv. Although there are other relatively large changes happening over short time periods in the record, the onset of the fall 2007 event is particularly fast, and the low transport values are sustained until the end of the record. This event will be explored in more detail in section 7.

[45] The relationships between changes in the PV of the different water masses and changes in the transport is such that the transport over the full extent of the section increases when PV is high in the dLSW layer, and negative at the OW depth range. As shown by others [e.g., *Kieke et al.*, 2006; *Rhein et al.*, 2011; *Peña-Molino et al.*, 2011], the evolution of upper and deep LSW also have opposite phase, since only one of the two types of water is formed in the Labrador Sea in a given winter. The EOF analysis finds that the export of recently ventilated uLSW is also associated with increased southwestward transport at Line W. In this scenario, our limited observational record suggests that enhanced convection in the Labrador Sea, the type that results in the production of dLSW, does not lead to a strengthening of the DWBC. It is the presence of recently ventilated OW, rather than LSW, that is associated with a stronger DWBC, similar to what is found in *Gerdes and Köberle*'s [1995] modeling work, among others. If the partition between interior and boundary current remains constant over time, a stronger DWBC would then translate into a stronger MOC, and enhanced convection in the Labrador Sea would not lead to a more vigorous MOC, as found by *Pickart and Spall* [2007]. However, changes in the NADW transport by the DWBC could also be in part compensated by changes in export via the interior pathways, leading to no change in the MOC.

[46] We note that this transport mode was obtained from a mode of variability that represents only 20% of the variability of the individual fields. How well does mode-derived transport compare with the total transports across the array? If we calculate the transports for the same layers using the full velocity and density fields from the ring/meander-free objectively mapped data (Figure 9, bottom), we find that the fluctuations in the total transport have shorter period than those captured by the mode, and the amplitudes are nearly twice as large. Nevertheless, the mode does a fair job at reproducing the low-frequency variability in the full record. Total transports, like the EOF1-derived transports, have no significant trend. However, there is some indication of a trend

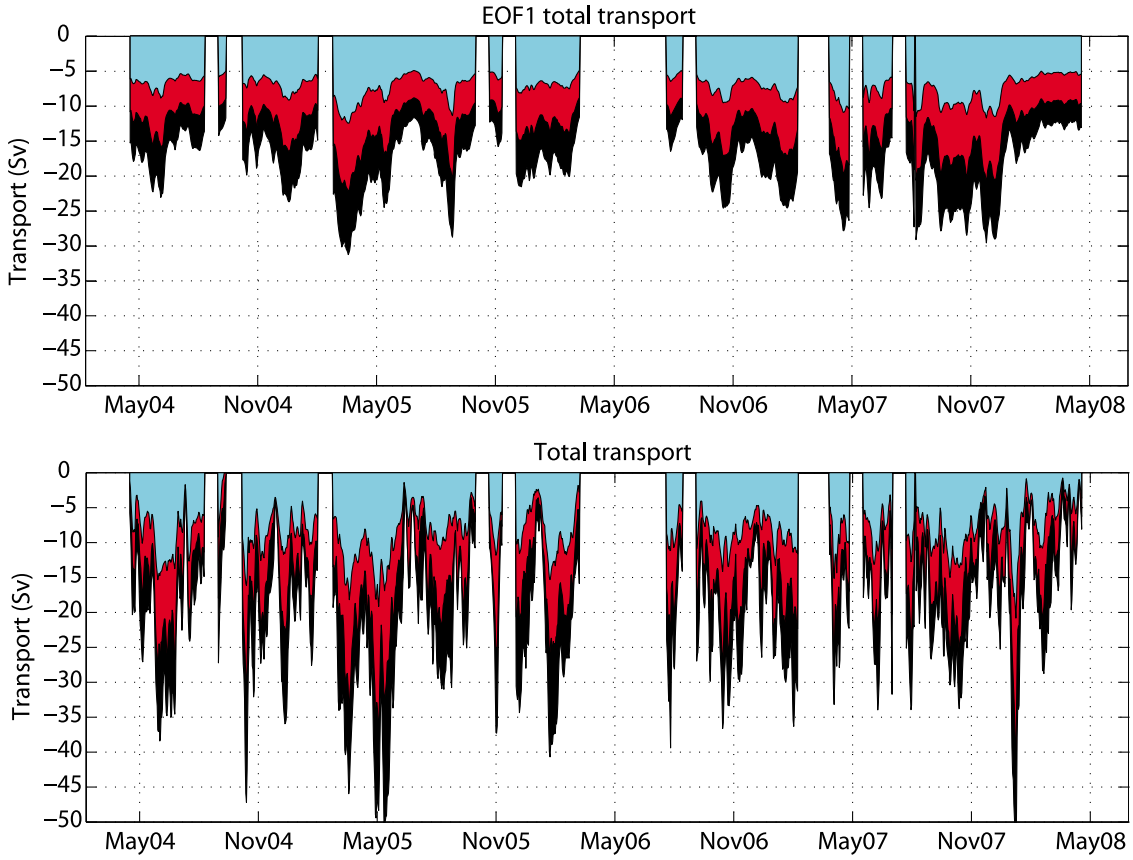

Figure 9. Transport, in sverdrups, integrated up to the maximum SW transport stream function for the dLSW, in blue, ISOW, in red, and DSOW in black. (top) The transport integrated from the combined EOF mode's density and downstream velocity fields. (bottom) The transport obtained using the full velocity field.

in the ratio between intermediate and deep-water masses, mostly reflecting the contribution from changes in layer thickness, which are much smaller than the other factors controlling the transport (average velocity and lateral extent).

[47] The amplitude of the EOF1-derived DWBC transport fluctuations presented here is in good agreement with the amplitude of the observed MOC variability: O(4 Sv) at Line W (standard deviation of the total transport, shown as the black area in Figure 9 (top)) versus O(5 Sv) at 26.5°N [e.g., *Cunningham et al.*, 2007; *Meinen et al.*, 2012]. However, the fraction of the MOC variability that is associated with changes in convective activity is most likely to be smaller, O(1–2 Sv) according to *Böning et al.* [2006] modeling results. Thus a fraction of our DWBC transport mode may still be associated with recirculations and therefore not contribute to the net southward transport of NADW at this latitude, but instead to the "leakyness" of the DWBC [*van Sebille et al.*, 2011].

7. The Winter 2007–2008 Rapid Event

[48] PC1 from the joint EOF analysis and the transport time series derived from it show a sudden change in the conditions during the winter of 2007–2008. In transport, this change is characterized by a drop of approximately 15 Sv distributed over the dLSW, ISOW and DSOW layers. In PV, this abrupt change is coincident with a redistribution from positive PV anomalies in the intermediate layers, and negative above and below, before the winter 2007–2008, to negative PV anomalies at intermediate depths, and positive above and below after. How exactly these changes affect the structure of the circulation at Line W can be better understood by looking at the sum of the velocity mode from the leading EOF before and after the winter of 2007–2008, that is EOF1 times the value of PC1 before and after the winter of 2007–2008, and the mean velocity section (Figure 10).

[49] There are two major changes taking place during this transition that can explain the sudden decrease in the transport. One is related to the north-south displacement of the Gulf Stream and the other one has to do with the reorganization of the flow around the deep and shallow DWBC velocity cores. Prior to the winter 2007–2008 (Figure 10, left), the Gulf Stream's North Wall, seen here as the transition from the negative to the positive downstream velocity, lays south of W5, beyond the array limits. The flow at the top of mooring W5 is to the southwest at this time. The largest velocities are found in the deepest of the velocity cores, slightly displaced offshore from its mean location at the bottom of W4 to the bottom of W5. The shallower of the deep cores, typically located around 2500 m, is weaker and somewhat isolated from the surrounding flow. The shallow velocity core is also weak. After the transition (Figure 10,

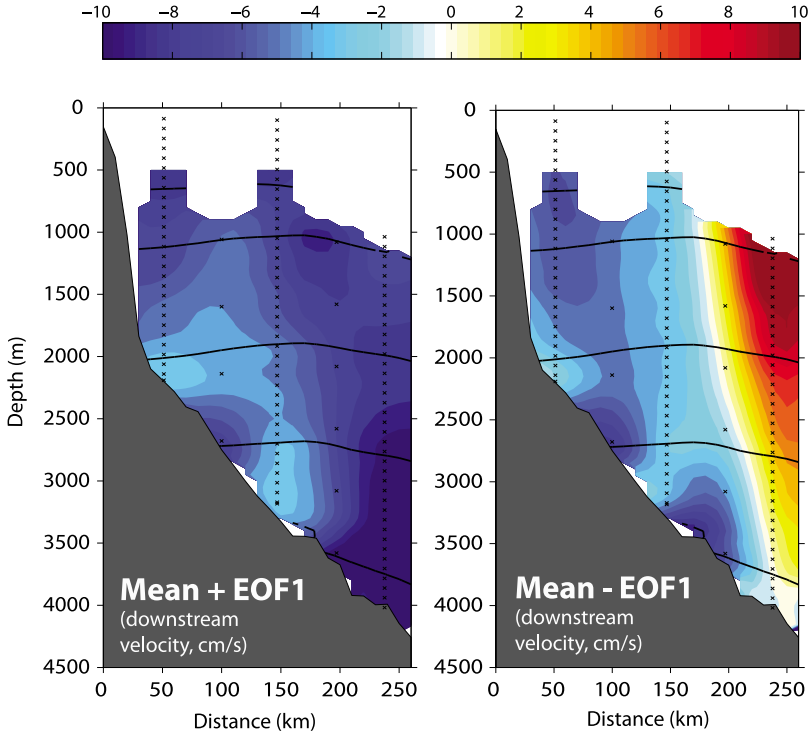

Figure 10. Total downstream velocity (left) before and (right) after the winter 2007–2008. These conditions are typical of all periods when PC1 is large and positive (mean + EOF1) or large and negative (mean − EOF1).

right), the northeastward flow in the deep Gulf Stream penetrates all the way to the bottom at W5 and the North Wall is now north of W4. In the upper part of the array, both the shallow and intermediate velocity cores intensified, and the flow becomes relatively barotropic everywhere north of W3. The deep core at the base of W4 is weaker and isolated from the rest of the southward flow.

[50] As a result of the changes in the position of the Gulf Stream and the associated reorganization of the deep flow, W4 and W5 experienced some of the largest velocity fluctuations in the entire array (Figure 7, top). The magnitude of these fluctuations can be seen in the integrated wavelet amplitude of the kinetic energy calculated from the original current meter data at W4 for different depths (Figure 11).

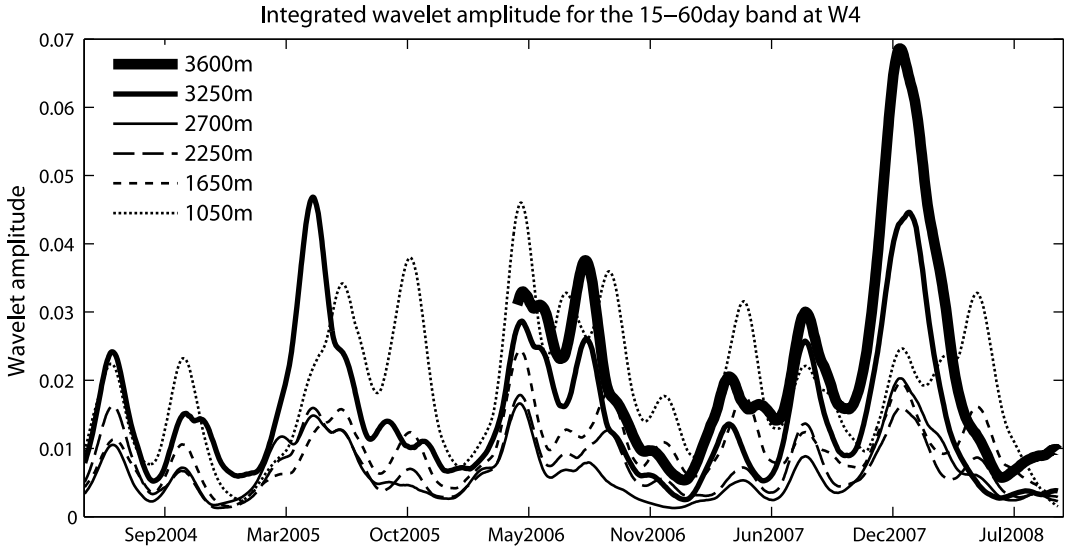

Figure 11. Integral of the wavelet amplitude of the kinetic energy from mooring W4 at different depths (no data for the bottom current meter were available for the first 2 years of the record). The energetic event during the winter of 2007–2008 has no corresponding peak in the ring/meander index (Figure 7, bottom).

The wavelet amplitude shows that motions are most energetic near the bottom, around the deep velocity core, and at the top of the mooring (~1000 m) right at the base of the surface intensified flow in the Gulf Stream. The peak in wavelet amplitude for the winter of 2007–2008 is the most energetic event in the record at W4 and in the whole array only exceeded by the large ring event in 2006 (see Figure 7).

8. Summary and Discussion

[51] The mean DWBC inferred from the Line W moored array observations for the period 2004–2008 consists of three distinct velocity cores: two bottom intensified features located at the base of the dLSW (~2500 m isobath) and the DSOW (~3500 m isobath), and a shallow one within the depth range of the uLSW approximately along the 2000 m isobath. These cores have typical velocities of 5–10 cm s^{-1} to the southwest, and are embedded in a background flow that is also directed to the southwest but with velocities that are weaker by a factor of 2. The southwestward flow in the DWBC is bounded offshore by the deep Gulf Stream, with velocities of a few centimeters per second to the northeast near the North Wall in the upper 2000 m of the water column. The Eulerian nature of these mean flows, together with the fact that the Gulf Stream is only partially sampled by Line W, are responsible for the small, compared to typical stream coordinate time mean Gulf Stream velocities in this area [*Johns et al.*, 1995; *Meinen et al.*, 2009], values reported here.

[52] The time series measured by the array documents energetic motions at a wide range of frequencies, with greater energy concentrated near the bottom and at the offshore end of the array. Velocity fluctuations near the bottom occur in the along-isobath direction with periods ranging from two weeks to two months, most likely associated with TRW generated by Gulf Stream instabilities. Rings and meanders, when present in the array, can cause fluctuations in the velocity and density fields that are 1 order of magnitude larger than the climate-related variability of the Slope Water and DWBC. Approximately 15% of the 4 year record at Line W is affected by them. The integrated effect of both rings and meanders in the 4 year record mean is a reduction of the southwestward flow across the array by a few sverdrups, flow that must be deflected offshore as shown by the *Bower and Hunt* [2000] float trajectories.

[53] When rings and meanders are excluded from the record, the principal mode of variability in the water mass composition that emerges from the joint EOF analysis of the velocity, temperature, salinity and PV consists of positive PV anomalies at intermediate depths confined between anomalies of the opposite sign in the water above and below. Using the smallness of the PV values as an indicator of recent ventilation [*Talley and McCartney*, 1982], we find that on average prior to 2006, the recently ventilated dLSW has a stronger presence at Line W (negative PV anomalies at intermediate depths). During this time, the uLSW and OW depth ranges are characterized by higher stratification values, and waters that are warmer and more saline than the mean, all indicative of lack of the ventilation. This out-of-phase behavior of the deep and upper LSW, the latter only partially resolved by the array, can be caused by changes in the forcing over the Labrador Sea. During harsh winters, typically positive NAO years, deep convection occurs and it leads to the formation of dLSW. When conditions are less severe, convection can still occur affecting shallower layers and only uLSW is formed [e.g., *Schott et al.*, 2004; *Yashayaev*, 2007]. The out-of-phase relation between the dLSW and the OW, on the other hand, can result from the same phase of the basin-scale atmospheric forcing acting on different regions of the North Atlantic [*Dickson et al.*, 1996]. During negative NAO years, air temperatures over the Greenland Sea are low, leading to larger heat fluxes (from the ocean to the atmosphere) and more ventilation of deep waters. In the Labrador Sea, low NAO years are associated with weaker than normal westerlies and reduced buoyancy forcing, inhibiting deep convection. Alternatively, this out-of-phase behavior between OW and LSW could also be the result of changes in the Labrador Sea alone, and the deepening of the interface between the dLSW and the OW being just a consequence of deep convection [*Sarafanov et al.*, 2009].

[54] In coordination with changes in the water mass distribution, we observe changes in the circulation that manifest in both the DWBC and the Gulf Stream. During phases when recently ventilated dLSW is present at the array, the deep flow (to the southwest) between the 1000 and the 3500 m isobaths increases, but the transport integrated across the DWBC decreases. This decrease in the transport is due to both a decrease in the lateral extent of the DWBC as well as a decrease in the southward flow in the deep water (offshore of the 3500 m isobath). Larger DWBC transports at Line W are associated with colder, fresher and weaker-stratified uLSW and OW, as often seen in modeling experiments [e.g., *Gerdes and Köberle*, 1995; *Böning et al.*, 1996; *Kohl and Stammer*, 2008].

[55] The expansion/contraction of the DWBC we observed is associated with north-south displacements of the Gulf Stream. These displacements can be of two types: (1) in phase north-south shift of the entire Gulf Stream axis and (2) changes in the meridional tilt of the Gulf Stream (they correspond to the first and second EOFs of the SSH-derived surface velocity in the western North Atlantic [*Peña-Molino*, 2010]). In particular, at Line W changes in the Gulf Stream position are mostly due to changes in its meridional tilt. When the Gulf Stream is south of its mean location at Line W, its path away from the separation point at Cape Hatteras is oriented more zonally, while a northerly Gulf Stream position corresponds to a more meridionally oriented path. Whether these changes in the Gulf Stream path are synchronized with changes in the water mass composition and velocity of the DWBC as a result of coordinated changes in their individual forcing, or they are a consequence of changes in the DWBC transport, is unclear from the data. However, some supporting evidence for the former is given by *Häkkinen and Rhines* [2009] analysis of the wind stress over the Slope Water. They showed that for the period of 2001–2005, the region between Cape Hatteras and the Nordic Sills was characterized by a positive curl which resulted in a more tilted zero curl line. These changes in the wind stress curl can drive changes in the path of the Gulf Stream as shown by *Kelly et al.* [1996]. Moreover, our PC1 presented here does not correlate well with the leading EOF of the Slope Water SST/circulation from *Peña-Molino and Joyce* [2008]. The Peña-Molino and Joyce Slope's surface temperature and velocity mode precedes in-phase north-south shifts of the entire Gulf Stream axis, rather than changes in

the meridional tilt of the current as seen at Line W. Changes in the tilt of the Gulf Stream only correlate with SST in certain areas of the Slope at zero lag [*Peña-Molino*, 2010].

[56] Fluctuations in the EOF-derived transport mode are similar in size to the observed variability of the MOC at 26.5°N [e.g., *Meinen et al.*, 2012], and suggest that the requirement for the velocity to be coupled to changes in the water mass properties implicit in the EOF analysis may be an effective way to filter out contributions to the MOC from forcings other than thermohaline. However, estimates of the temporal variability of the partition between deep-water export by the DWBC versus the interior do not exist at the present time, and it cannot be ruled out that a certain compensation between these two pathways may exist leading to a smaller contribution by the DWBC than that reported here.

[57] The analysis of two additional years of data from the central mooring at Line W, W3, acquired prior to the full array deployment *Peña-Molino et al.*, 2011], suggested that the changes described here are part of a longer-term change in the DWBC water mass composition from a dLSW-dominant period in the early 2000s to a uLSW- and OW-dominant period in the later part of the decade. This gradual trend was interrupted suddenly during the winter of 2007–2008, coinciding with the reestablishment of deep convection in the Labrador Sea [*Våge et al.*, 2009; *Yashayaev and Loder*, 2009]. The beginning of the trend reversal was marked by very energetic velocity fluctuations near the bottom of the deeper moorings. The frequency and vertical trapping of these motions are typical of topographic Rossby waves. However, unlike the rest of the TRW-like fluctuations that are present in the record, this particular event was the only one unrelated to Gulf Stream rings and meanders. Clearly, TRW are not only forced by Gulf Stream instabilities. The work by *Hallberg and Rhines* [1996] showed that the response to thermohaline forcing in a basin with sloping boundaries occurred mostly via topographic Rossby waves. Along the sloping boundary, the topographic β effect is much larger than the planetary β, so the waves propagate along the boundary leaving the shallow water to the right, downstream in the DWBC sense. *Gascard and Clarke* [1983] observed TRW in the Labrador Current within the Labrador Sea during the winter and hypothesized these waves were the response of the horizontal velocity field to deep convection. So it is possible that these energetic motions that we see at W4 are part of the response to deep convection in the Labrador Sea that occurred in the winter of 2007–2008, and as they propagate, they cause changes in the circulation of the western North Atlantic that affect both the Gulf Stream and the DWBC. According to *Roussenov et al.* [2008] the topographic wave response to changes in the Labrador Sea could be felt in the western North Atlantic as fast as 1 month after the forcing began. In the work of *Gerdes and Köberle* [1995], this rapid response via topographic waves is only the first stage of the two-stage adjustment to the thermohaline forcing in the Nordic seas; it is followed by a much slower response during the second stage that is caused by the advection of the modified dense water properties. The gradual trend and the rapid response we see at Line W could manifest such a two-stage adjustment. However, if this is the case, our record is not sufficiently long to observe the slow advective response to the most recent convective activity which, based on the spreading rates of the LSW that was ventilated in the mid-1990s and early 2000s [*van Sebille et al.*, 2011; *Peña-Molino et al.*, 2011], could take up to 9 years.

[58] **Acknowledgments.** Financial support for the Line W program (2004–2008) was provided by the U.S. National Science Foundation (grants OCE-0241354 and OCE-0726720) as well as funding from the WHOI's Ocean and Climate Change Institute. We would also like to thank Amy S. Bower, Michael A. Spall and John Marshall for their comments on an earlier version of this work, as well two anonymous reviewers for their contribution to the final version of the manuscript.

References

Böning, C. W., F. O. Bryan, W. R. Holland, and R. Doscher (1996), Deep-water formation and meridional overturning in a high-resolution model of the North Atlantic, *J. Phys. Oceanogr.*, *26*, 1142–1164.

Böning, C. W., M. Scheinert, J. Dengg, A. Biastoch, and A. Funk (2006), Decadal variability of subpolar gyre transport and its reverberation in the North Atlantic overturning, *Geophys. Res. Lett.*, *33*, L21S01, doi:10.1029/2006GL026906.

Bower, A. S., and H. D. Hunt (2000), Lagrangian observations of the Deep Western Boundary Current in the North Atlantic Ocean. Part I: Large-scale pathways and spreading rates, *J. Phys. Oceanogr.*, *30*, 764–783.

Bower, A. S., S. Lozier, and S. Gary (2011), Export of Labrador Sea Water from the subpolar North Atlantic: A Lagrangian perspective, *Deep Sea Res., Part II*, *58*, 1798–1818, doi:10.1016/j.dsr2.2010.10.060.

Brown, O. B., P. C. Cornillon, S. R. Emmerson, and H. M. Carle (1986), Gulf Stream warm rings: A statistical study of their behavior, *Deep Sea Res., Part A*, *33*, 1459–1473.

Clarke, R. A., and J.-C. Gascard (1983), Formation of Labrador Sea water. Part I: Large-scale processes, *J. Phys. Oceanogr.*, *13*, 1764–1778.

Cronin, M., and D. R. Watts (1996), Eddy-mean flow interaction in the Gulf Stream at 68°W. Part I: Eddy energetics, *J. Phys. Oceanogr.*, *26*, 2107–2131.

Csanady, G. T., and P. Hamilton (1988), Circulation of slopewater, *Cont. Shelf Res.*, *8*, 565–624.

Cunningham, S. A., et al. (2007), Temporal variability of the Atlantic meridional overturning circulation at 26.5°N, *Science*, *317*, 935–938, doi:10.1116/science.1141304.

Curry, R. G., and M. S. McCartney (2001), Ocean gyre circulation changes associated with the North Atlantic Oscillation, *J. Phys. Oceanogr.*, *31*, 3374–3400.

Dickson, R., J. Lazier, J. Meincke, P. Rhines, and J. Swift (1996), Long-term coordinated changes in the convective activity of the North Atlantic, *Progress Oceanogr.*, *38*, 241–295.

Eden, C., and J. Willebrand (2001), Mechansism of interannual to decadal variability of the North Atlantic circulation, *J. Clim.*, *14*, 2266–2280.

Fratantoni, P. S., and R. S. Pickart (2003), Variability of the shelf break jet in the Middle Atlantic Bight: Internally or externally forced?, *J. Geophys. Res.*, *108*(C5), 3166, doi:10.1029/2002JC001326.

Gary, S. F., M. S. Lozier, C. Böning, and A. Biastoch (2011), Deciphering the pathways for the deep limb of the Meridional Overturning Circulation, *Deep Sea Res., Part II*, *58*, 1781–1797.

Gascard, J.-C., and R. A. Clarke (1983), Formation of labrador sea water. Part II: Mesoscale and smaller-scale processes, *J. Phys. Oceanogr.*, *13*, 1779–1797.

Gerdes, R., and C. Köberle (1995), On the influence of DSOW in a numerical model of the North Atlantic general circulation, *J. Phys. Oceanogr.*, *25*, 2624–2642.

Häkkinen, S., and P. B. Rhines (2009), Shifting surface currents in the northern North Atlantic Ocean, *J. Geophys. Res.*, *114*, C04005, doi:10.1029/2008JC004883.

Halkin, D., and T. Rossby (1985), The structure and transport of the Gulf Stream at 73°W, *J. Phys. Oceanogr.*, *15*, 1439–1452.

Hallberg, R., and P. Rhines (1996), Buoyancy-driven circulation in an ocean basin with isopycnals intersecting the sloping boundary, *J. Phys. Oceanogr.*, *26*, 913–940.

Johns, W. E., T. J. Shay, J. M. Bane, and D. R. Watts (1995), Gulf Stream structure, transport, and recirculation near 68°W, *J. Geophys. Res.*, *100*, 817–838.

Joyce, T., et al. (1983), Rapid evolution of a Gulf Stream warm-core ring, *Nature*, *308*, 837–840, doi:10.1038/308837a0.

Joyce, T. M., J. Dunworth-Baker, R. S. Pickart, D. Torres, and S. Waterman (2005), On the Deep Western Boundary Current south of Cape Cod, *Deep Sea Res., Part II*, *52*, 615–625.

Kelly, K. A., M. J. Caruso, and S. Singh (1996), Observations of atmosphere-ocean coupling in midlatitude, *J. Geophys. Res.*, *101*, 6295–6312.

Kieke, D., M. Rhein, L. Stramma, W. M. Smethie, D. A. Lebel, and W. Zenk (2006), Changes in the CFC inventories and formation rates of upper Labrador Sea Water, 1997–2001, *J. Phys. Oceanogr.*, *36*, 64–86.

Kohl, A., and D. Stammer (2008), Variability of the meridional overturning in the North Atlantic from the 50-year GECCO state estimation, *J. Phys. Oceanogr.*, *38*, 1913–1930.

Koltermann, K. P., A. V. Sokov, V. P. Terescenlov, S. A. Dobroliubov, K. Lorbacher, and A. Sy (1999), Decadal changes in the thermohaline circulation of the North Atlantic, *Deep Sea Res., Part II*, *46*, 109–138.

Lazier, J. R. N. (1980), Oceanographic conditions at ocean weather ship Bravo, 1964–1974, *Atmos. Ocean*, *18*(3), 227–238.

Lindstrom, S. S., and D. R. Watts (1994), Vertical motion in the Gulf Stream near 68°W, *J. Phys. Oceanogr.*, *24*, 2321–2333.

Macrander, A., U. Send, H. Valdimarsson, S. Jónsson, and R. H. Käse (2005), Interannual changes in the overflow from the Nordic Seas into the Atlantic Ocean through Denmark Strait, *Geophys. Res. Lett.*, *32*, L06606, doi:10.1029/2004GL021463.

Mauritzen, C., and S. Häkkinen (1999), On the relationship between dense water formation and the Meridional Overturning Cell in the North Atlantic Ocean, *Deep Sea Res., Part I*, *46*, 877–894.

Meinen, C. S., D. S. Luther, and M. O. Baringer (2009), Structure, transport and potential vorticity of the Gulf Stream at 68°W: Revisiting older data sets with new techniques, *Deep Sea Res., Part I*, *56*, 41–60, doi:10.1016/j.dsr.2008.07.010.

Meinen, C. S., W. S. Johns, S. L. Garzoli, E. van Seville, D. Rayner, T. Kanzow, and M. O. Baringer (2012), Variability of the Deep Western Boundary Current at 26.5°N during 2004–2009, *Deep Sea Res., Part II*, doi:10.1016/j.dsr2.2012.07.036, in press.

North, G. F., T. L. Bell, R. F. Cahalan, and F. J. Moeng (1982), Sampling errors in the estimation of empirical orthogonal functions, *Mon. Weather Rev.*, *110*, 699–706.

Peña-Molino, B. (2010), Variability in the North Atlantic Deep Western Boundary Current: Upstream causes and downstream effects as observed at Line W, PhD thesis, MIT/WHOI Jt. Program in Phys. Oceanogr., Woods Hole, Mass.

Peña-Molino, B., and T. M. Joyce (2008), Variability in the Slope Water and its relation to the Gulf Stream path, *Geophys. Res. Lett.*, *35*, L03606, doi:10.1029/2007GL032183.

Peña-Molino, B., T. M. Joyce, and J. M. Toole (2011), Recent changes in the Labrador Sea Water within the Deep Western Boundary Current southeast of Cape Cod, *Deep Sea Res., Part I*, *58*, 1019–1030, doi:10.1016/j.dsr.2011.07.006.

Pickart, R. S. (1994), Interaction of the Gulf Stream and the Deep Western Boundary Current where they cross, *J. Geophys. Res.*, *99*, 25,155–25,164.

Pickart, R. S. (1995), Gulf Stream-generated topographic Rossby waves, *J. Phys. Oceanogr.*, *25*, 574–586.

Pickart, R. S., and W. M. Smethie (1993), How does the Deep Western Boundary Current cross the Gulf Stream?, *J. Phys. Oceanogr.*, *23*, 2602–2616.

Pickart, R. S., and M. A. Spall (2007), Impact of Labrador Sea convection on the North Atlantic Meridional Overturning Circulation, *J. Phys. Oceanogr.*, *37*, 2207–2227, doi:10.1175/JPO3178.1.

Pickart, R. S., and D. R. Watts (1990), Deep Western Boundary Current variability at Cape Hatteras, *J. Mar. Res.*, *48*, 765–791.

Rayner, D., et al. (2011), Monitoring the Atlantic meridional overturning circulation, *Deep Sea Res., Part II*, *58*, 1744–1753, doi:10.1016/j.dsr2.2010.10.056.

Rhein, M., D. Kieke, S. Hüttl-Kabus, A. Roessler, C. Mertens, R. Meissner, B. Klein, C. W. Böning, and I. Yashayaev (2011), Deep water formation, the subpolar gyre, and the meridional overturning circulation in the subpolar North Atlantic, *Deep Sea Res., Part II*, *58*, 1819–1832, doi:10.1016/j.dsr2.2010.10.061.

Roussenov, V. M., R. G. Williams, C. W. Hughes, and R. J. Bingham (2008), Boundary wave communication of bottom pressure and overturning changes for the North Atlantic, *J. Geophys. Res.*, *113*, C08042, doi:10.1029/2007JC004501.

Rossby, T., and E. Gottlieb (1998), The Oleander Project: Monitoring the variability of the Gulf Stream and adjacent waters between New Jersey and Bermuda, *Bull. Am. Meteorol. Soc.*, *79*(1), 5–18.

Sarafanov, A., A. Falina, H. Mercier, P. Lherminier, and A. Sokov (2009), Recent changes in the Greenland-Scotland overflow-derived water transport inferred from hydrographic observations in the southern Irminger Sea, *Geophys. Res. Lett.*, *36*, L13606, doi:10.1029/2009GL038385.

Schott, F. A., R. Zantopp, L. Stramma, M. Dengler, J. Fischer, and M. Wibaux (2004), Circulation and deep-water export at the western exit of the subpolar North Atlantic, *J. Phys. Oceanogr.*, *34*, 817–843.

Schott, F. A., M. Dengler, R. Zantopp, L. Stramma, J. Fischer, and P. Brandt (2005), The shallow and Deep Western Boundary Circulation of the South Atlantic at 5–11°S, *J. Phys. Oceanogr.*, *35*, 2031–2053.

Schott, F. A., J. Fischer, M. Wibaux, M. Dengler, and R. Zantopp (2006), Variability of the Deep Western Boundary Current east of the Grand Banks, *Geophys. Res. Lett.*, *33*, L21S07, doi:10.1029/2006GL026563.

Shay, T. J., J. M. Bane, D. R. Watts, and K. L. Tracey (1995), Gulf Stream flow field and events near 68°W, *J. Geophys. Res.*, *100*, 22656–22589.

Silverthorne, K. E., and J. M. Toole (2009), Seasonal kinetic energy variability of near-inertial motions, *J. Phys. Oceanogr.*, *39*, 1035–1049, doi:10.1175/2008JPO3920.1.

Stommel, H., and A. B. Arons (1960), On the abyssal circulation of the world ocean—I. Stationary planetary flow patterns on a sphere, *Deep Sea Res.*, *6*, 140–154.

Talley, L. D., and M. S. McCartney (1982), Distribution and circulation of Labrador Sea water, *J. Phys. Oceanogr.*, *12*, 1189–1204.

Talley, L. D., J. L. Reid, and P. E. Robbins (2003), Data-based meridional overturning stream functions for the global ocean, *J. Clim.*, *16*, 3213–3226.

Thompson, R. (1971), Topographic rossby waves at a site north of the Gulf Stream, *Deep Sea Res.*, *18*, 1–19.

Thompson, R., and J. R. Luyten (1976), Evidence for bottom-trapped topographic Rossby waves from signal moorings, *Deep Sea Res.*, *23*, 629–635.

Toole, J. M., R. G. Curry, T. M. Joyce, M. McCartney, and B. Peña-Molino (2011), Transport of the North Atlantic Deep Western Boundary Current about 39N, 70W: 2004–2008, *Deep Sea Res., Part II*, *58*, 1768–1780, doi:10.1016/j.dsr2.2010.10.058.

Torrence, C., and G. P. Compo (1998), A practical guide to wavelet analysis, *Bull. Am. Meteorol. Soc.*, *79*(1), 61–78.

Våge, K., R. S. Pickart, V. Thierry, G. Reverdin, C. M. Lee, B. Petrie, T. A. Agnew, A. Wong, and M. H. Ribergaard (2009), Surprising return of deep convection to the subpolar North Atlantic Ocean in winter 2007–2008, *Nat. Geosci.*, *2*, 67–72, doi:10.1038/ngeo382.

van Sebille, E., M. O. Baringer, W. E. Johns, C. S. Meinen, L. M. Beal, M. Femke de Jong, and H. M. van Aken (2011), Propagation pathways of classical Labrador Sea water from its source region to 26°N, *J. Geophys. Res.*, *116*, C12027, doi:10.1029/2011JC007171.

Watts, D. R., and W. E. Johns (1982), Gulf Stream meanders: Observations on propagation and growth, *J. Geophys. Res.*, *87*, 9467–9476.

Wunsch, C. (2006), *Discrete Inverse State Estimation Problems*, Cambridge Univ. Press, Cambridge, U. K.

Yashayaev, I. (2007), Hydrographic changes in the Labrador Sea, 1960–2005, *Progress Oceaongr.*, *73*, 242–276.

Yashayaev, I., and J. W. Loder (2009), Enhanced production of Labrador Sea Water in 2008, *Geophys. Res. Lett.*, *36*, L01606, doi:10.1029/2008GL036162.